Design Procedure for a Very High Speed Slotless Permanent Magnet Motor

Pierre-Daniel Pfister, *Student Member, IEEE* and Yves Perriard, *Senior Member, IEEE*

Laboratory of Integrated Actuator (LAI)
Ecole Polytechnique Fédérale de Lausanne (EPFL)
1015 Lausanne, Switzerland

***Abstract*— The paper presents a very high speed slotless permanent magnet motor design procedure using an analytical model. The multiphysics analytical model allows a quick optimization process using a sequential quadratic programming method. The presented model includes the magnetic fields, the mechanical stresses in the rotor, the electromagnetic power losses, the windage power losses and the power losses in the bearings. The paper also presents an example of optimization.**

I. Introduction

Due to their high power density, very high speed (VHS) permanent magnet (PM) motors are increasingly demanded on the market [1].

In a VHS motor, the different parts and the different materials are pushed to their thermal and mechanical limits. Indeed, as the speed is very high, high stresses appear in the rotor. As the mechanical power is given by $P = T\omega$, for a given output power P at high speeds ω one needs a much lower torque T and volume than at lower speeds. Hence, there is a high power density. This article shows an innovative procedure to VHS PM motors design.

II. The necessity of a multiphysics fully analytical model

The mechanical optimum for the motor would be to reduce the rotor diameter to diminish the stress in it, but it would reduce the motor torque. The magnetic optimum would be to reduce the air gap, but it would increase the windage power losses. These two simple examples show us the importance of having an optimization which uses the complete multiphysics model of the system.

In the considered case finite elements methods are extremely heavy for optimization processes. Therefore an analytical model is used. The model is applied to the motor structure shown in Fig. 1. Our geometry is: a magnet at the center, a sleeve, an air gap, the coils, and the stator yoke.

III. The analytical model

A. The magnetostatic fields

To solve the field, the polar coordinate system (r, α) is used. Magnetic field in the PM is calculated using Poisson's equation:

$$\nabla^2\phi = \frac{\nabla \cdot \vec{B}_R}{\mu_0\mu_r} \quad (1)$$

with $\vec{B}_R$ the PM remanent field, μ_r the relative permeability, μ_0 the free space permeability and ϕ the scalar magnetic potential. The magnetic fields in the sleeve, the air, and the coils are calculated by setting $\vec{B}_R = 0$ in (1), which gives Laplace's equation. The hypothesis of infinite permeability in the yoke is made.

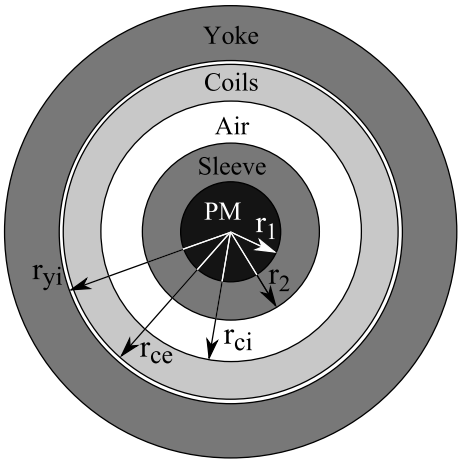

Fig. 1. Motor structure

Xia and Zhu's article [2] resolves the two equations in the following geometry: a shaft in the center, a magnet, an air gap, and the stator yoke. In our case, the shaft radius is set to zero. The radial radial field B_r in the air gap is obtained:

$$B_r(r,\alpha) = \hat{B}_r(r)\cos p(\alpha-\theta) \quad (2)$$

with

$$\hat{B}_r(r) = \frac{2B_R p}{1+p}\frac{\left[\left(\frac{r}{r_{yi}}\right)^{p-1}\left(\frac{r_1}{r_{yi}}\right)^{p+1}+\left(\frac{r_1}{r}\right)^{p+1}\right]}{\left[(1+\mu_r)+(1-\mu_r)\left(\frac{r_1}{r_{yi}}\right)^{2p}\right]} \quad (3)$$

and with p the number of pole pairs, μ_r the magnet relative permeability, r_1 the outer radius of the magnet, r_{yi} the inner radius of the stator yoke, θ the rotor orientation.

We calculate Laplace's torque T acting on the copper with the current density J:

$$T = \int_{coil} rJB_r(r,\alpha)\mathrm{d}\tau \quad (4)$$

with $\mathrm{d}\tau$ an element of volume.

The result is the following:

$$T = \frac{2B_R J l_a r_1^{p+1} \left[\frac{r_{ce}^{p+2} - r_{ci}^{p+2}}{r_{yi}^{2p}(p+2)} + g(p, r_{ce}, r_{ci}) \right] f(\alpha_i, \theta, p)}{(1+p)\left[(1+\mu_r) + (1-\mu_r)\left(\frac{r_1}{r_{yi}}\right)^{2p} \right]} \tag{5}$$

with l_a the active length, r_{ce} the outer radius of the coil, r_{ci} the inner radius of the coil, and

$$g(p, r_{ce}, r_{ci}) = \begin{cases} \frac{r_{ce}^{-p+2} - r_{ci}^{-p+2}}{-p+2} & \text{if } p \in \mathbb{N}^* \setminus \{2\} \\ \ln\left(\frac{r_{ce}}{r_{ci}}\right) & \text{if } p = 2 \end{cases} \tag{6}$$

and

$$\begin{aligned} f(\alpha_i, \theta, p) = & \sin(p(\alpha_4 - \theta)) - \sin(p(\alpha_3 - \theta)) \\ & - (\sin(p(\alpha_2 - \theta)) - \sin(p(\alpha_1 - \theta))) \end{aligned} \tag{7}$$

with α_i $i = 1, ..., 4$ the angles which set the dimensions of one coil.

B. Mechanical stresses

The mechanical stresses (σ_r, σ_α) in the rotor are calculated using the equilibrium equation [3]:

$$\frac{\mathrm{d}\sigma_r}{\mathrm{d}r} + \frac{\sigma_r - \sigma_\alpha}{r} + F_r = 0 \tag{8}$$

with F_r the radial force density. Hook's law gives the dependence of the strain ε on the stresses:

$$\varepsilon_r = \frac{1}{E}(\sigma_r - \nu\sigma_\alpha) \tag{9}$$

$$\varepsilon_\alpha = \frac{1}{E}(\sigma_\alpha - \nu\sigma_r) \tag{10}$$

with E Young's modulus and ν poisson's ratio.

In a rotating system a volume element is subject to the following force F:

$$F = \rho\omega^2 r \tag{11}$$

with ω the anglular velocity.

Using the following values, we obtain the results shown on Fig. 2:

$$\begin{aligned} \nu_s &= 0.32 \\ \nu_m &= 0.3 \\ \omega &= 2\ \pi\ 3333\ \ \mathrm{s}^{-1} \\ \rho_s &= 4.42 \times 10^3\ \ \frac{\mathrm{kg}}{\mathrm{m}^3} \\ \rho_m &= 7.7 \times 10^3\ \ \frac{\mathrm{kg}}{\mathrm{m}^3} \\ E_s &= 116 \times 10^9\ \ \frac{\mathrm{N}}{\mathrm{m}^2} \\ E_m &= 150 \times 10^9\ \ \frac{\mathrm{N}}{\mathrm{m}^2} \\ e_0 &= 2 \times 10^{-5}\ \ \mathrm{m} \\ r_1 &= 5.80 \times 10^{-3}\ \ \mathrm{m} \\ r_2 &= 6.21 \times 10^{-3}\ \ \mathrm{m} \end{aligned}$$

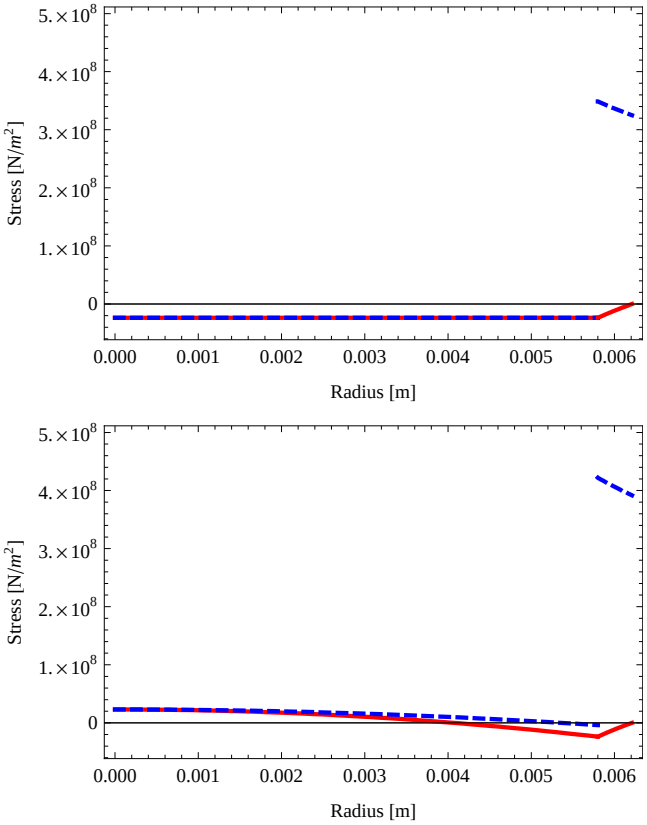

Fig. 2. Radial (continuous line) and tangential stress (dashed line) in the magnet and the sleeve along a radius. Top: stresses at no speed (tangential and radial stresses have the same value in the PM). Bottom: Stresses at 200 krpm.

with ν_s and ν_m Poisson's ratio respectively of the sleeve and of the magnet, ρ_s and ρ_m the density of the sleeve and the magnet, E_s and E_m Young modulus of the sleeve and the magnet, e_0 the radial interference between the magnet and the sleeve, r_1 and r_2 the outer radius of the magnet and the sleeve.

The permanent magnet is fragile. In order that it does not break at high speeds, it is prestressed, as shown on Fig. 2 (top): at no speed, the radial and tangential stresses are negative in the PM. The limiting factors are the radial stress at the center, and the tangential stress at the inner side of the sleeve at high speeds: Fig. 2 (bottom).

C. Thermal model

The steady state temperature T is calculated using the heat diffusion equation [4]:

$$k\nabla^2 T + \dot{q} = \rho c_p \frac{\partial T}{\partial t} \tag{12}$$

with k the thermal conductivity, ρ the material density, $\dot{q}$ the rate at which thermal energy is generated per unit of volume and c_p the specific heat.

Because of the 3D thermal interactions in the motor, and because of the air movements in the air gap, this 2D thermal model is not consistent with the reality. It is used to give us

indications and not to constraint the model. Further investigations in the thermal modeling need to be done.

So the thermal aspect of the motor is not directly taken into account. But, as the motor is designed by minimizing the total power losses, the thermal aspect is indirectly taken into account.

D. Electromagnetic power losses

Joule power losses density p_{cop} in the coils is calculated as:

$$p_{cop} = \rho_c J^2 \tag{13}$$

with ρ_c the resistivity and J the current density.

The stator iron power losses P_{iron} are assumed to be generated only by the PM. Their density p_{iron} is calculated approximately using Steinmetz equation:

$$p_{iron} = c_1 f^{c_2} \hat{B}^{c_3} \tag{14}$$

with c_i, $i = 1, 2, 3$ being empirical coefficients, $\hat{B}$ the maximum magnetic field and f the frequency. The same empirical approach used in [5] for the hysteresis power losses is used here for the iron power losses.

The eddy current and hysteresis power losses in the magnet are neglected. The eddy currents in the sleeve and in the coils are also neglected.

E. Windage power losses

The article from Vrancik [6] indicates us that the windage power losses P_w are calculated as:

$$P_w = \pi C_d l r_2^4 \omega^3 \rho_{air} \tag{15}$$

with l the length considered, r_2 the inner radius of the air gap, ω the angular velocity and ρ_{air} the air density. The skin friction coefficient C_d is calculated using an empirical formula:

$$\frac{1}{\sqrt{C_d}} = 2.04 + 1.768 \ln(Re\sqrt{C_d}) \tag{16}$$

with Re the Reynolds number.

Fig. 3 shows the windage power losses given by this model for an air gap length of 34 mm when the motor turns at 200 krpm.

F. Mechanical power losses in the bearings

The power losses in the bearings $P_{bearings}$ [7] can be estimated by:

$$P_{bearings} = c_4 \omega^{c_5} \tag{17}$$

with c_4 and c_5 be two empirical constants.

In our case, ceramic ball bearing are used.

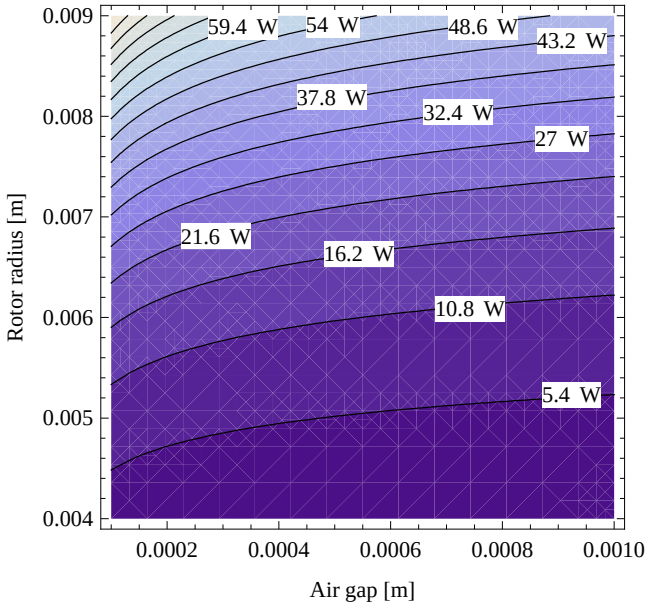

Fig. 3. Windage power losses in an air gap cylinder of 34 mm of length at 200 krpm.

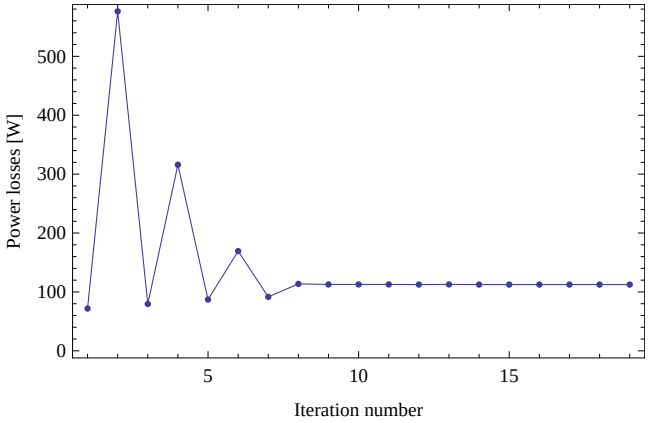

Fig. 4. Representation of the objective function (the power losses) for each iteration.

IV. Optimization procedure

The model contains more than 140 equations and 190 variables. The system has 13 degrees of freedom. The commercial software *Pro@Design* is used to perform the optimization [8]. This program is based on a sequential quadratic programming (SQP) solver using the partial derivatives and penalty functions. One parameter is chosen to be the objective function and all the others are fixed, constrained in intervals or free.

Fig. 4 shows the minimization of the objective function which is in our case the total power losses. One can note that the minimum value of power losses shown on the graphic is in this example at the first iteration. The algorithm does not converge to this value of losses because some constraints are not satisfied at this iteration.

V. Optimization example

Because of the mechanical normal modes, the active length of the motor was constrained to be smaller or equal to 30 mm. The motor specifications are:

Active length of the motor (l_a)	$\leq$30	mm
PM remanence (B_R)	1.18	T
Number of phases	3	
Mechanical power	2	kW
Speed	200	krpm

The optimal design generated by Pro@Design is:

Active length of the motor (l_a)	30	mm
Outer radius of the PM (r_1)	5.80	mm
Outer radius of the sleeve (r_2)	6.21	mm
Outer radius of the coils (r_{ce})	14.14	mm
Number of pole pairs (p)	1	
Phase current amplitude (sin wave)	36.25	A
Efficiency	94.5	%
Bearing power losses ($P_{bearings}$)	53	W
Joule power losses (P_{cop})	39	W
Air gap power losses (P_w)	11	W
Iron power losses (P_{iron})	13	W

VI. Discussion

The optimization process showed in our case that:

1) It is very fast: it takes only a few seconds to find the optimum.
2) A 2 pole pairs motor needs to have a bigger active length than a 1 pole pair one to reach the optimum efficiency, which is problematic with respect to the mechanical normal modes. Concerning the control electronics, the solution with 1 poles pair is also more suitable.
3) Without any constraints on the active length, the optimization process finds an optimal design without sleeve with an active length of $l_a = 61.69$ mm and an outer radius of the PM of $r_1 = 5.06$ mm.

Some important models are still missing: a vibration model, a model of the electronics, a model of the power losses in the PM, the sleeve, and the coils due to the variation of the magnetic field. The power losses in the yoke should be refined taking into account the field created by the coils.

VII. Prototype

A prototype has been designed using this analytical model. It is shown on Fig. 5. Although it is designed for 200 krpm and 2 kW, some construction constraints are added to the presented constraints in the optimization process. In means that the prototype is slightly different compared to the optimization example.

The prototype is being measured and the results will be shown in more details in a future publication. Nevertheless, the first results already showed the benefits of the analytical approach. The prototype designed using the analytical model showed better results than the previous prototypes. It already reached 200 krpm.

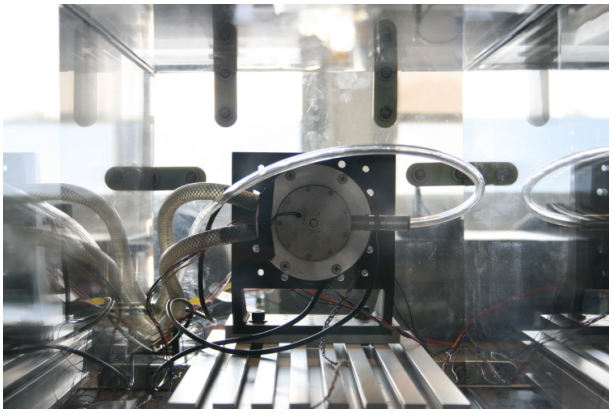

Fig. 5. Test and measurement bench for the high speed prototype.

VIII. Conclusion

The optimization procedure presented in the paper enables to quickly obtain the optimal design. Different materials, motor configurations, and constraints for the motor parameters are tested.

IX. Acknowledgment

The authors want to thank *Moving Magnet Technologies SA* and *Sonceboz SA* for their support. They also want to thank B. Reudet for his great help in the prototyping process.

References

[1] M. Rahman, A. Chiba, and T. Fukao, "Super high speed electrical machines - summary," *2004. IEEE Power Engineering Society General Meeting*, pp. 1272–1275, 2004.

[2] Z. Xia, Z. Zhu, and D. Howe, "Analytical magnetic field analysis of halbach magnetized permanent-magnet machines," *IEEE Transactions on Magnetics*, vol. 40, pp. 1864–1872, 2004.

[3] A. Bazergui, T. Bui-Quoc, A. Biron, G. McIntyre, and C. Laberge, *Résistance des matériaux, troisième édition*. Presses internationales polytechniques, 2002.

[4] F. Incropera and D. DeWitt, *Fundamentals of heat and mass transfer, fourth edition*. New York: John Wiley & Sons, 1996.

[5] P.-D. Pfister, C. Koechli, M. Markovic, and Y. Perriard, "Analysis of hysteresis losses in synchronous permanent magnet motors," in *Electromagnetic Field Computation, 2006 12th Biennial IEEE Conference on*, 2006, p. 144.

[6] J. Vrancik, "Prediction of Windage Power Loss in Alternators," NASA, Tech. Rep., 1968.

[7] K. Tanimoto, K. Kajihara, and K. Yanai, "Hybrid ceramic ball bearings for turbochargers." *SAE Transactions: Journal of Materials & Manufacturing*, vol. 109, pp. 763–775, 2000.

[8] "Pro@design optimization software." [Online]. Available: http://www.designprocessing.com/